Article

Lithium Ion Batteries—Development of Advanced Electrical Equivalent Circuit Models for Nickel Manganese Cobalt Lithium-Ion

Alexandros Nikolian *, Yousef Firouz, Rahul Gopalakrishnan, Jean-Marc Timmermans, Noshin Omar, Peter van den Bossche and Joeri van Mierlo

Department Mobility, Logistics and Automotive Technology Research Centre, Vrije Universiteit Brussels, Pleinlaan 2, Brussels 1050, Belgium; yousef.firouz@vub.ac.be (Y.F.); rgopalak@vub.ac.be (R.G.); jean-marc.timmermans@vub.ac.be (J.-M.T.); noshomar@vub.ac.be (N.O.); pvdbos@vub.ac.be (P.v.d.B.); joeri.van.mierlo@vub.ac.be (J.v.M.)

* Correspondence: alexandros.nikolian@vub.ac.be; Tel.: +32-2629-3620

Abstract: In this paper, advanced equivalent circuit models (ECMs) were developed to model large format and high energy nickel manganese cobalt (NMC) lithium-ion 20 Ah battery cells. Different temperatures conditions, cell characterization test (Normal and Advanced Tests), ECM topologies (1st and 2nd Order Thévenin model), state of charge (SoC) estimation techniques (Coulomb counting and extended Kalman filtering) and validation profiles (dynamic discharge pulse test (DDPT) and world harmonized light vehicle profiles) have been incorporated in the analysis. A concise state-of-the-art of different lithium-ion battery models existing in the academia and industry is presented providing information about model classification and information about electrical models. Moreover, an overview of the different steps and information needed to be able to create an ECM model is provided. A comparison between begin of life (BoL) and aged (95%, 90% state of health) ECM parameters (internal resistance (R_o), polarization resistance (R_p), activation resistance (R_{p2}) and time constants (τ) is presented. By comparing the BoL to the aged parameters an overview of the behavior of the parameters is introduced and provides the appropriate platform for future research in electrical modeling of battery cells covering the ageing aspect. Based on the BoL parameters 1st and 2nd order models were developed for a range of temperatures (15 °C, 25 °C, 35 °C, 45 °C). The highest impact to the accuracy of the model (validation results) is the temperature condition that the model was developed. The 1st and 2nd order Thévenin models and the change from normal to advanced characterization datasets, while they affect the accuracy of the model they mostly help in dealing with high and low SoC linearity problems. The 2nd order Thévenin model with advanced characterization parameters and extended Kalman filtering SoC estimation technique is the most efficient and dynamically correct ECM model developed.

Keywords: lithium ion; nickel manganese cobalt (NMC); equivalent circuit model (ECM); validation profile; modelling; begin of life (BoL) parameters; cell characterization; dynamic discharge pulse test (DDPT); worldwide harmonized light vehicle test procedure (WLTC)

1. Introduction

Academic research and applications of lithium-ion batteries have seen a growth in interest during the past decade [1–19]. This is mainly due to the increased use of applications ranging from small to high energy and power demanding systems [4], stationary applications encompassing grid energy storage, uninterruptible power supply and renewable power management systems [20]. The automotive industry is investing in the research and development of electric vehicles (EV) based on

new batteries and driveline technologies to transition their market from fully internal combustion engine (ICE) to a more environmental and efficient fleet of hybrid electric vehicles (HEVs), plug-in electric vehicles (PEVs) which encompass extended range electric vehicles (EREV), plug-in hybrid electric vehicles (PHEVs) and battery electric vehicles (BEVs) [1–3,21–23]. The development of EREV and PHEV electric applications has led to vastly different required battery properties regrading both the power and energy needed in these type of vehicles, compared to conventional HEVs and pure BEVs. The development of lithium-ion batteries to fulfil these demanding properties and in this way enable these type of vehicles has been a great achievement.

Thus, to understand and to control the behavior of the battery in terms of its chemical, electrical and thermal aspects during the different operational conditions is of high importance. Moreover equivalent circuit model (ECM) models not only are needed to manage the cells inside a battery pack with the battery management system (BMS), but also for the development and creation of efficient and proper battery packs [24–26]. The jump from an individual cell to a battery pack needs proper development and correct power, energy and heat management design and operation [24].

In this paper, an initial overview of the different lithium-ion battery models found in the literature is presented. The cell chemistry under investigation is a pouch nickel manganese cobalt (NMC) 20 Ah lithium ion with a nominal voltage 3.65 V as seen in Table 1. The manufacturer of these cells is EIG (Cheonan, South Korea) and all the characteristics mentioned in Table 1 are taken from the datasheet of the C020 model, available on the company website [27].

Table 1. Characteristics of the nickel manganese cobalt (NMC) cell.

Characteristics	Values	Unit
Length	217	(mm)
Width	130	(mm)
Thickness	7.1	(mm)
Weight	428	(g)
Nominal voltage	3.65	(V)
Nominal capacity	20	(Ah)
Specific energy	174	(Wh/Kg)
Energy density	370	(Wh/L)
Specific power	2300	(W/Kg)
Power density	4600	(W/L)

The analysis starts by providing a concise state-of-the-art of lithium ion battery models. A categorization of these models is proposed and further information regarding electrical models is presented. The analysis continues with a summary of the different tasks and activities performed before the creation of electrical models. A review of the various parameters used for the creation of the ECM models is included continuing with the overview of the different electrical models based on ECM topologies of the NMC chemistry at different temperatures conditions and validation profiles. The models developed have been created with two types of state of charge (SoC) estimation techniques, Coulomb counting and extended Kalman filtering.

2. Overview of the State of the Art of Lithium Ion Models

Investigating the scientific literature regarding the modelling of lithium-ion batteries behavior, it is found that different models have been already created and used for the different interdisciplinary sciences based on battery system operation. The different types of existing models can be separated mainly by the different issues and phenomena the model should investigate. In Table 2 the different model types have been separated into:

- Electrochemical models;
- Electrical models;

- Thermal models;
- Mechanical/fatigue models;
- Interdisciplinary models.

Table 2. Classification of different lithium-ion models [28]. ECM: equivalent circuit models; RC: combination of resistances and capacitance; PNGV: partnership for a new generation of vehicles.

Model Type		Model	Empirical	Semi-Empirical	Physical
Electro-chemical		Pure electro-chemical	-	-	√
		ECM electro-chemical	-	√	-
Electrical	Analytical	Peukert's model	√		-
		Rakhmatov and vrudula	-	√	-
		Sheperd other iterations	-	√	-
	ECM	State space	√	-	-
		Simple rint	√	-	-
		Enhanced rint	-	√	-
		RC	-	√	-
		PNGV/FreedomCAR	-	√	-
		1st Order (thevenin model)	-	√	-
		2nd Order (thevenin model)	-	√	-
		Enhanced PNGV (2nd order)	-	√	-
		Noshin model	-	√	-
		Neural nets	√		-
	Frequency	Frequency domain	√	√	-
Thermal		Analytical thermal	-		√
		ECM Thermal	-	√	-
Mechanical/Fatigue		Fatigue/Mechanical	-	√	√
Combined models		Electro-thermal	-	√	-
		Thermo-electrochemical	-	√	√
		Thermo-mechanical	-	√	√

When modelling the behavior of a physical system, it is possible to identify three main general model categories. Depending on the method how the inputs are related to the outputs of the model they can be categorized in: empirical, physical and semi-empirical models [29].

Empirical models are based on the "black-box" approach, where the inner physical behavior of the system is unknown and the relations between the inputs and outputs of the model are only based on experimental results and relations.

An example of the empirical models is the neural network model, which can capture the dynamic behavior of the battery and learn the relationship between the inputs to the outputs only through experimental data found prior to the creation of the model. Another example of empirical modelling of batteries is the analytical model called Peukert's model which can simulate the time needed to discharge the battery and to investigate the discharge rate capability of a battery. The main constants of the mathematical equation governing the Peukert's model have to be defined with the use of experimental activities [30,31].

Physical models are based solely on theoretical and physical knowledge of the system under investigation. No experimental activities regarding the relation between the inputs and outputs of the system have to be performed in order to determine the behavior of your system. Depending on the knowledge of the specific inner characteristics and physical process of the system a model can be created to simulate the performance of your system. An example of a physical model of a lithium-ion battery is the pure electrochemical model [32–34]. Depending on the knowledge of the specific material composition and the properties of the chemical reactions, a set of physical equations were originally developed [35,36]. The fact that the model equations are based on physical relations, which describe real physical effects taking place in the battery, includes the pure electrochemical model in the category of physical modelling.

Finally, semi-empirical models lay between the physical and the empirical models. This category is a hybrid modelling category. The system under investigation is to a certain extent treated as a black-box where the relation of the inputs to your outputs and inner behavior of the system is investigated

through experimental methods, as performed for empirical modelling. The difference being that, a link with some of the real physical effects inside the system can be implemented in the model. Examples of semi-empirical models are ECMs (e.g., dual polarization, partnership for a new generation of vehicles (PNGV)) that can be linked to in this case to the polarization effect and the different behavior during charging and discharging processes [9,14,19,28,37,38]. The models implemented to simulate the NMC cells for this publication belong to the semi-empirical model category. These kind of models are mainly created for the beginning of life (BoL) of cells were ageing phenomena have not yet affected the creation of the model parameters. When including in these type of models ageing phenomena to be echoed in the parameters created from the characterization tests the development of more advanced models is performed, thus diverging from the definition of semi-empirical models.

2.1. Battery Management System

Electric applications using a battery as their primary energy (*i.e.*, a BEV) and a power source (*i.e.*, HEV), will be typically accompanied by a BMS. This is mostly implemented in vehicle applications where the need to manage the battery performance, control internal parameters of the battery and inform the user of vital battery information is needed. The accurate prediction of SoC, state of heath and other characteristics (temperature, voltage, and current) are the main needed information to be calculated by a BMS. In addition, the proper management of the charging and discharging behavior of the battery by the BMS, will help to maintain for a longer period the rated capacity of the battery and increase its lifetime. This will keep the battery in good operating and stable conditions for a longer period. Thus, it is very important for the BMS software to be based on a battery model, which can calculate efficiently and accurate the battery states and characteristics and can run with low computational power and time [39].

2.2. Electrical Models

Models that describe the electrical behavior of the battery have been extensively studied and developed in academia [19,40–45]. There exist multiple models that can be used to describe the electrical response of the battery and in this study those have been categorized as follows:

- Analytical models;
- Electrical ECM models;
- Frequency domain models.

Electrical models are mainly semi-empirical models where characterization techniques are performed to identify the different parameters of the battery. Those characterization techniques have been extensively described in different standardization documents [44–49] and they are generally composed of:

- Capacity test: defining the discharge/charge capacity of the battery;
- Open circuit voltage (OCV) *versus* SoC test: relating the SoC levels with the open circuit voltage of the battery;
- Hybrid pulse power characterization (HPPC) test: to define the internal resistances and SoC of the battery;
- Electrochemical impedance spectroscopy (EIS) test: define the internal resistance and impedance of the battery.

2.3. Creation of an Electrical Equivalent Circuit Model

In Figure 1, a schematic representation is presented showing the different theoretical steps that have to be taken to achieve a complete development of a model and validate it afterwards. Initially, the choice of the electrical model to use should be considered carefully. Depending on the model chosen, the creation of appropriate parameters have to be developed to represent the different components

of the ECM model. These parameters would be collected and re-arranged in the appropriate format to create a lookup table, which would be in function of current, SoC, temperature and lifetime. Implementing correctly the variables inside the model would provide the required information to the model to simulate the behavior of the studied lithium ion cells. Based on these parameters a preliminary simulation can be performed taking as validation profile the different pulses performed during the HPPC test. This preliminary analysis can be observed for the 0.5 C pulse at the 70% SoC level in Figure 2. This comparison show us that the analysis of the characterization results can be correctly and easily performed while it gives the possibility to check the parameters created for each SoC level of the HPPC test.
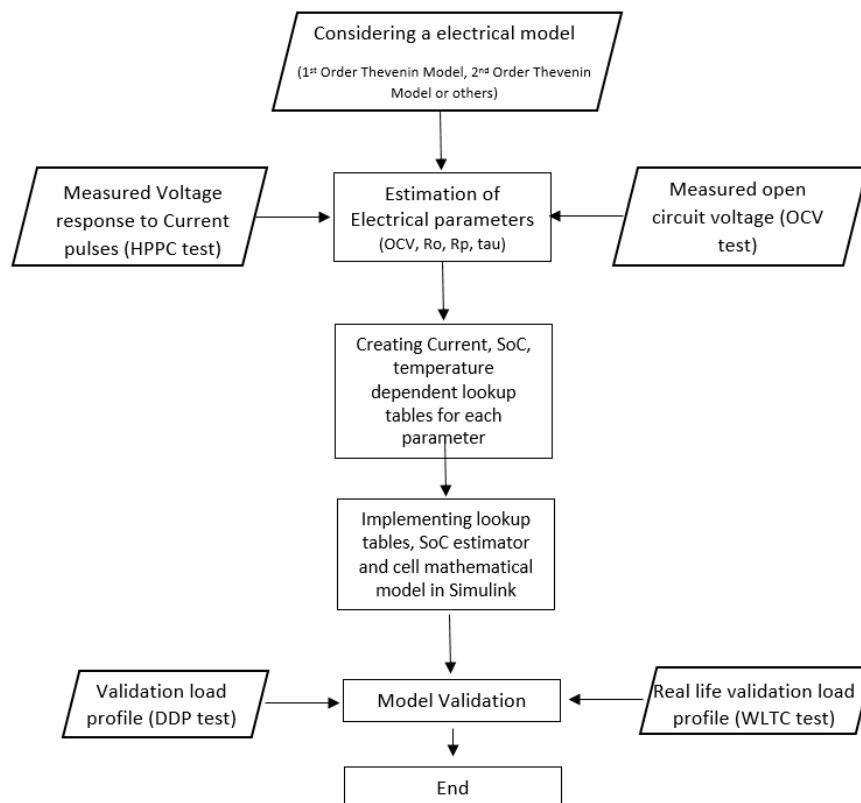
Figure 1. Schematic representation of the activities to create an equivalent circuit model (ECM) model.
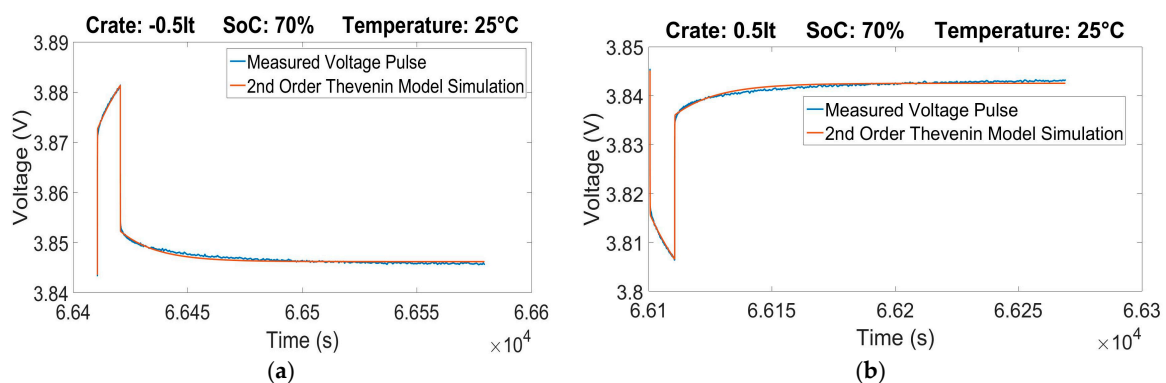
Figure 2. Measured voltage *vs.* simulated voltage during the 0.5 °C rate pulse at the 70% state of charge (SoC) level of a hybrid pulse power characterization (HPPC) test at 25 °C: (**a**) Charge pulse; and (**b**) discharge pulse.

In this paper the ECM topologies used during the simulations performed are the 1st order and 2nd order Thévenin battery models. The 1st order Thévenin battery model consists of a resistance (internal resistance (R_o)) connected to a branch in series, which consists of a second resistance (polarization resistance (R_p)) in parallel with a capacitor (polarization capacitor (C_p)). The 2nd order Thévenin model, which in theory should be more accurate than the 1st order Thévenin battery model consists of a resistance (internal resistance (R_o)) connected with two parallel branches in series. Each branch incorporates a resistance and a capacitor simulating the chemical behavior of the cell. The first branch is composed of an activation resistance and capacitor while the second one is composed of a concentration resistance and a capacitor. In Table 3 a list of the different parameters needed for the parameterization of the ECM models is presented. From this table, we can observe the difference in required number of parameters between the 1st and 2nd order Thevenin model. In particular, the polarization resistance and time constants of the 1st order Thevenin model are separated in the activation and concentration chemical behavior of the cell in the case of the 2nd order Thevenin model.

Table 3. List of parameters for 1st and 2nd order Thevenin Models. OCV: open circuit voltage; R_o: internal resistance; R_p: polarization resistance; R_{pa}: activation resistance; R_{pc}: concentration resistance; t_p: polarization time-constant; t_{pa}: activation time-constant; t_{pc}: polarization time-constant.

Model Parameters	1st Order Thevenin	2nd Order Thevenin	Units
OCV	$\checkmark$	$\checkmark$	(V)
R_o	$\checkmark$	$\checkmark$	(mOhms)
R_p	$\checkmark$	-	(mOhms)
R_{pa}	-	$\checkmark$	(mOhms)
R_{pc}	-	$\checkmark$	(mOhms)
t_p	$\checkmark$	-	(s)
t_{pa}	-	$\checkmark$	(s)
t_{pc}	-	$\checkmark$	(s)

2.4. State of Charge Estimation

The calculation of the correct SoC during simulation of any battery model is a key issue and is of great importance to determine the correct characteristics of the battery and to achieve good results [50–54]. Specifically, battery models that are to be implemented in BMS systems for automotive and stationary applications need to estimate the SoC of the battery pack with high accuracy. In parallel, a proper BMS system implemented with a very accurate SoC estimator could be affected by the required high computational power and runtime.

There exist different types of techniques for determining the actual SoC [55]. These different methods can be separated into experimental and adaptive techniques. This categorization is also utilized when describing the different techniques used in state-of-health (SoH) estimations [54]. The experimental technique, which is a function of capacity, current and temperature called the Coulomb counting technique [9]. The adaptive technique is called Kalman filtering and takes into consideration the output (simulated voltage) and input (load current and temperature) of the model to recalculate and update the SoC value in the model value back to the model [56]. In this study a more advanced technique is used which is the extended Kalman filtering [16,53,57].

The Coulomb counting SoC estimation technique has been used extensively in the literature [50,56,58–60] and can be used to determine and update the battery cells SoC during simulations. It counts the charge transferred from or to the battery in order to calculate the remaining available capacity, expressed as the SoC [54]. The proper implementation of the measured capacity values from the capacity test allows calculating the SoC through Coulomb counting technique in an accurate way. The Coulomb counting equation is described in Equation (1):

$$z\left(t\right) = z\left(t_0\right) - \frac{1}{3600C} \int_{t_0}^{t} I\left(t\right) \mathrm{d}t \tag{1}$$

where:

$z(t)$: The SoC at time t;
$z(t_0)$: Initial SoC (at time t = t_0);
C: Estimated battery cell available capacity as function of temperature, current rate and charge/discharge state (Ah);
$I(t)$: Battery current (A) assumed positive when discharging.

In general, the concept behind Kalman filtering is that, at each time step, an initial prediction of the state vector is made, which is used to predict the corresponding model output (*i.e.*, the terminal voltage) [61,62]. The true terminal voltage is then measured and compared to the battery model output. Based on the error and output noise covariance, the predicted state vector is optimally corrected via the Kalman gain to obtain the corrected or posterior state estimate [16]. It is important to mention that, in contrast to the Coulomb counting-based SoC estimation, the Kalman filter-based SoC estimation, also requires a voltage measurement.

3. Results

3.1. Comparison of Aged and Begin of Life 2nd Order Thévenin Model Parameters for Nickel Manganese Cobalt Battery Cells

The SoH of a battery cell has been defined as the health condition of a battery at a reference temperature and a reference current rate. The battery 100% SoH corresponds to the BoL state of a fresh cell (available discharge capacity) and the 0% SoH corresponds with the end of life (EoL) of the battery. As a general rule it is accepted in the automotive industry that the 80% SoH is the EoL of the battery [46,63]. In Equation (2), the SoH relation with the measured capacity and the initial capacity of a cell is given:

$$\text{SoH} = 100 \times \frac{C_{\text{measured}}}{C_{\text{initial}}} \tag{2}$$

where:

C_{actual}: measured available discharge capacity (Ah);
C_{initial}: Initial available discharge capacity (Ah).

The SoH of a battery pack inside an automotive application is being calculated through the BMS. By calculating the SoH of the battery cells used we can quantify the level of aging of the cell, which is caused by a capacity fade and/or power fade. Thus having the possibility to understand at which point it would be more appropriate to replace the battery cells. This analysis can be also applied to the different parameters that are created when performing ECM modelling activities to observe their variation.

A state of health analysis on all the parameters utilized to simulate the 2nd order Thévenin model has been performed. The comparison of the parameters was conducted at 45 °C. By choosing a high temperature to compare our parameters we can observe parameters that are affected by increased aging phenomena due to the extreme temperature condition. In Figure 3, the behavior of the capacity values can be observed as a function of the number of full equivalent cycles. It is observed that the capacity values are slightly increasing for the initial 200 equivalent cycles but as the cell, further ages the total available discharge capacity is decreasing. The capacity values of the cell have been determined by performing a capacity test at recommended manufacturer C-rate (0.5 C). Every 100 equivalent cycles the cell performs a series of characterization tests including the capacity test, OCV and HPPC test. From an initial capacity value of 20.03 Ah for the fresh cell, we note a decreased value to 18.05 Ah after 700 equivalent cycles. This corresponds to a SoH level of 90.11%.
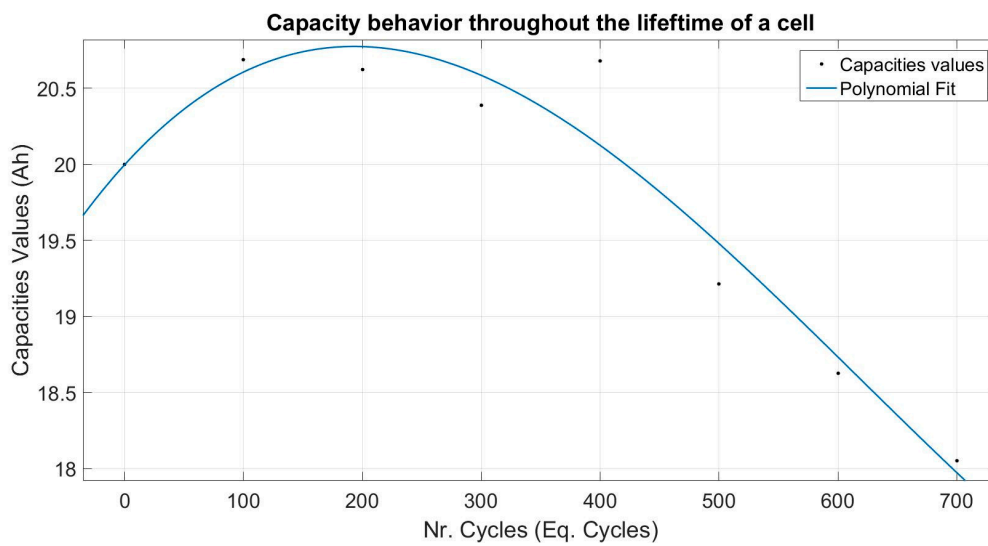
Figure 3. Capacity behavior of a lithium ion cell throughout its lifetime.

The OCV difference between an aged and new battery cell is presented in Figure 4. Due to the small difference between the BoL OCV and the aged OCV in Table 4, the absolute difference between the lines is calculated. A higher difference can be observed between the discharge than the charge BoL and aged OCV curves. It should be noted that the discharge/charge capacity should differ between the aged and the fresh battery cell due to ageing phenomena. This effect is not reflected in Figure 4 as the SoC is used instead, to plot the evolution of the OCV.

Table 4. SoC-OCV values for charge and discharge for a fresh and aged (90% state-of-health (SoH)) NMC 20 Ah.

Charge SoC (%)	Charge ΔV (mV)	Discharge SoC (%)	Discharge ΔV (mV)
0	10.00	100	10.00
2	2.97	98	13.91
4	5.88	96	13.88
6	6.62	94	14.83
8	4.93	92	15.79
10	4.98	90	16.63
15	5.82	85	16.59
20	5.80	80	17.59
25	5.22	75	21.15
30	2.55	70	31.58
35	1.57	65	18.13
40	0.49	60	12.93
45	0.24	55	10.94
50	0.71	50	9.49
55	1.89	45	9.51
60	2.20	40	10.96
65	1.45	35	14.02
70	3.62	30	13.74
75	0.10	25	11.92
80	1.73	20	12.41
85	0.22	15	11.83
90	3.07	10	11.61
92	3.99	8	13.25
94	5.00	6	16.78
96	6.77	4	17.35
98	7.48	2	13.48
100	8.00	0	10.00

Continuing the analysis on the battery models parameters, it should be noted that the values presented in Figures 5–7 are from parameters, which are a function of SoC, current rate, expressed in C-rate and temperature. In the cases of the battery models parameters the 95% SoH values are also presented. The values observed are the mean value of the parameters for all C-rates at which the HPPC was performed at each SoC level. Due to the complex representation, the time constants graph (Figure 8) incorporates the total value of the τ_1 and τ_2. It should be noted that the value of τ_1 are much lower than the values of τ_2. Moreover the creation of the R_o, R_p and R_{p2} parameters are more easily created because they are based on the behaviour of a resistance while the values τ_1 and τ_2 are based on a capacitor behaviour which is more difficult to simulate [14,64].
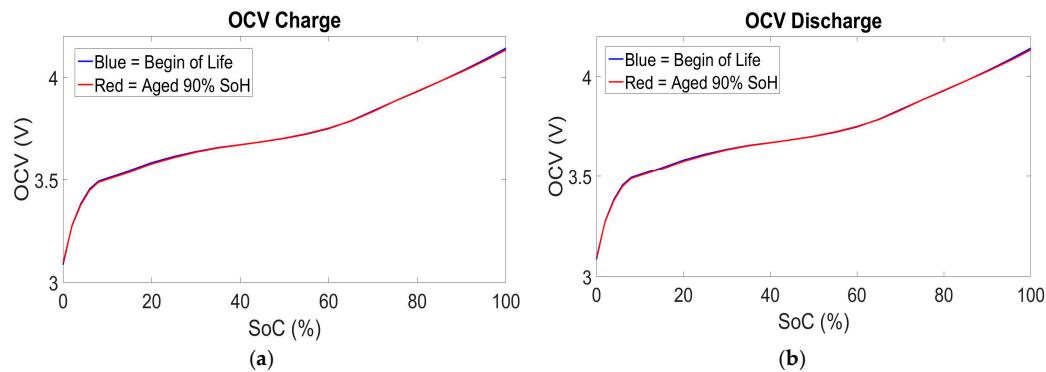
Figure 4. OCV difference between a fresh begin of life (BoL) and aged (90% SoH) lithium ion cell: (**a**) OCV charge; and (**b**) OCV discharge.
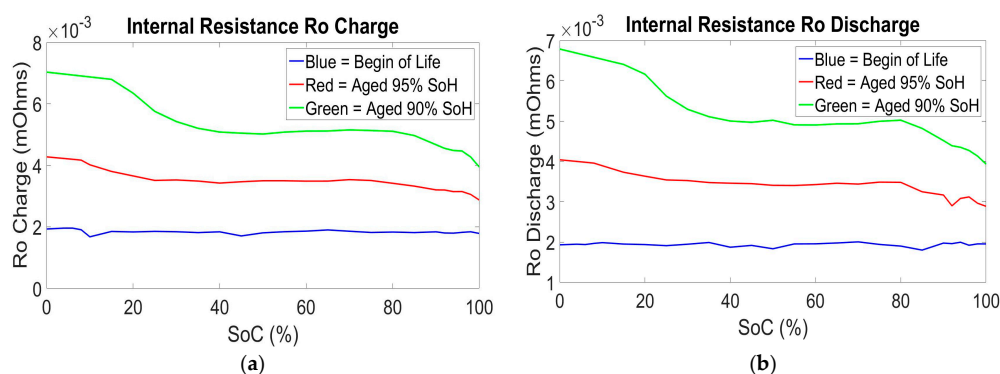
Figure 5. R_o difference between a fresh BoL and aged (95% and 90% SoH) lithium ion cell: (**a**) R_o charge; and (**b**) R_o discharge.
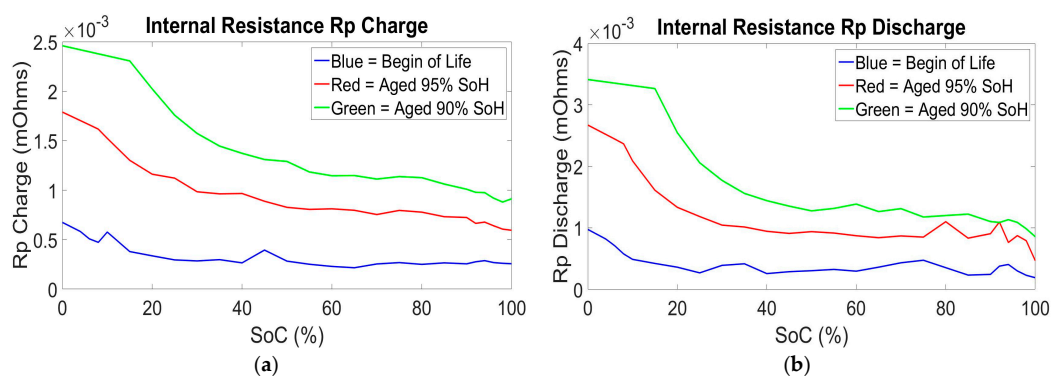
Figure 6. Activation R_p difference between a fresh BoL and aged (95% and 90% SoH) lithium ion cell: (**a**) R_p charge; and (**b**) R_p discharge.
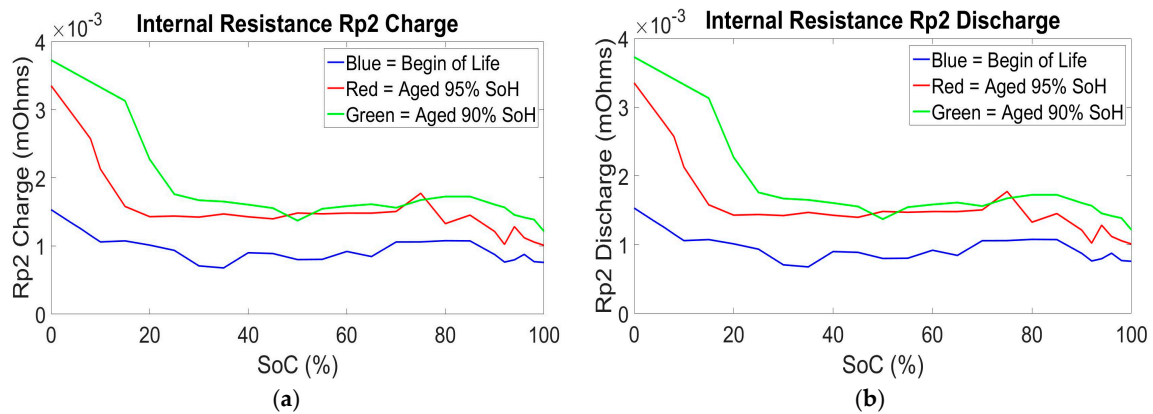
Figure 7. Concentration R_{p2} difference between a fresh BoL and aged (95% and 90% SoH) lithium ion cell: (**a**) R_{p2} charge; and (**b**) R_{p2} discharge.
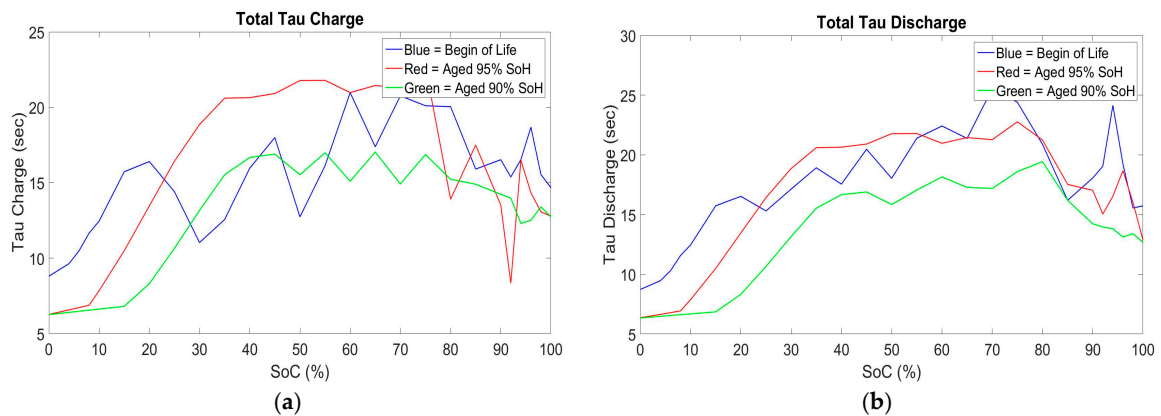
Figure 8. Total time constants (τ) difference between a fresh BoL and aged (95% and 90% SoH) lithium ion cell: (**a**) Total τ charge; and (**b**) total τ discharge.

In Figure 9 the internal resistance under 1 current rate for different temperatures (15 °C, 25 °C, 35 °C and 45 °C) is shown to represent the temperature dependency of the parameter. The behavior of the parameters is as expected having a higher resistance for low temperatures and lower as one goes to higher temperatures [65].
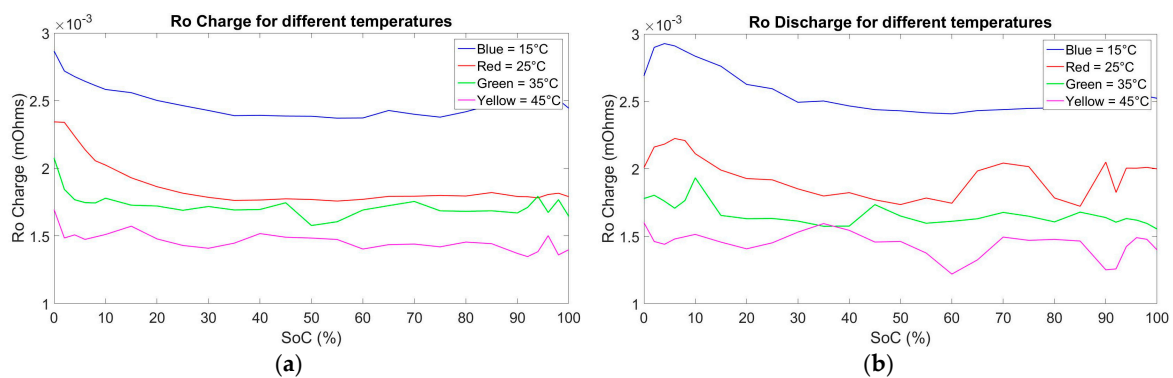
Figure 9. Internal resistance (R_o) for different temperatures (15 °C, 25 °C, 35 °C and 45 °C): (**a**) R_o charge; and (**b**) R_o discharge.

3.2. Equivalent Circuit Model Nickel Manganese Cobalt Models

As mentioned previously, a set of ECM models have been created to simulate the behavior of the battery cell under different ECM topologies, validation profiles and temperatures conditions. In addition different SoC estimation techniques (Coulomb counting and extended Kalman Filter) are incorporated into the battery models.

The battery models created are based on parameters calculated from two types of characterization tests. Normal and advanced characterization tests have been developed to acquire a better understanding of the high and low SoC levels battery cell behaviors. The normal characterization tests consists of performing a specific test (*i.e.*, HPPC, OCV-SoC) at each 5% step of the total SoC while advanced characterization tests consists of separating the total SoC window into three parts where the high SoC's (100% to 90%) and the low SoC's levels (10% to 0%) tests are performed in 2% steps of the SoC while the middle SoC's (90% to 10%) with 5% steps. Two types of ECM topologies were utilized, the 1st order and the 2nd order Thévenin battery models. The extended Kalman filtering technique was applied only on the 2nd order Thévenin battery model while it was the only topology that was validated with the more dynamic profile called the worldwide harmonized light vehicle test procedure (WLTC). With the exception of the WLTC, the validation of all models were created from 15 °C, 25 °C, 35 °C and 45 °C.

Only the battery models at 25 °C for each category is being shown while a table showing the validation errors (Tables 5–8) for each temperature is incorporated at the end of each category. For each battery models (25 °C 1st and 2nd order Thevenin models with dynamic discharge pulse test (DDPT) and WLTC validation profiles Coulomb counting and extended Kalman filtering SoC estimation technique) presented the first figure (Figures 10, 13, 16, 19, 22) where the whole SoC window simulation results is shown. This is followed by the figures where the validation errors are revealed (Figures 11, 14, 17, 20, 23). The error is calculated according to the Equation 3 below. For each model, a third figure (Figures 12, 15, 18, 21, 24) is included where we can observe the dynamic behavior of the model created.

$$\text{err \%} = 100 \times \frac{V_{\text{measured}} - V_{\text{simulated}}}{V_{\text{measured}}} \tag{3}$$
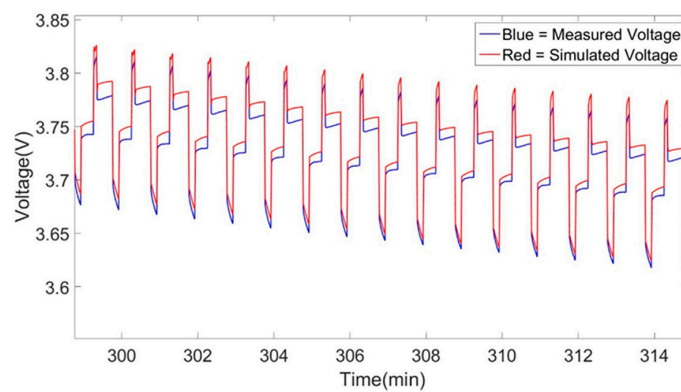
3.2.1. 1st Order Thévenin Model with Normal Characterization
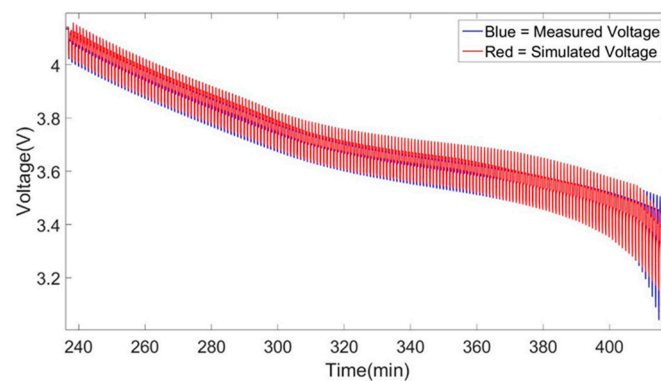
Figure 10. 1st order Thévenin model measured and simulated dynamic discharge pulse (DDP) comparison at 25 °C with Coulomb counting and normal characterization.
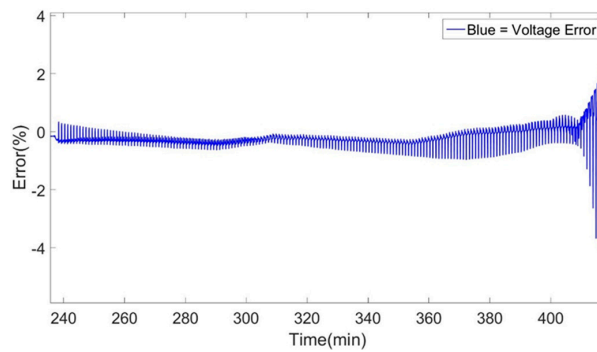
Figure 11. Error of the 1st order Thévenin model measured and simulated DDP comparison at 25 °C with Coulomb counting and normal characterization.
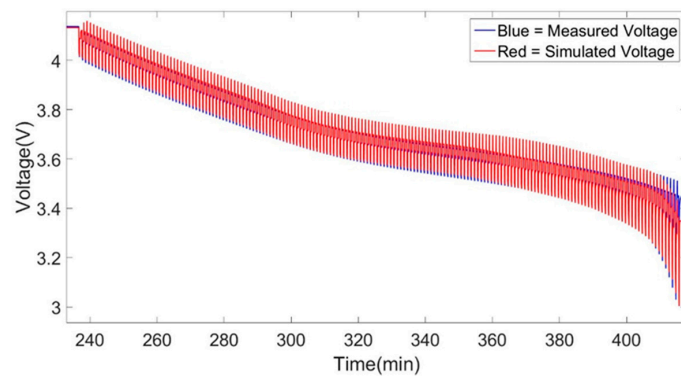

Figure 12. Dynamic behavior of the 1st order Thévenin Model measured and simulated DDP comparison at 25 °C with Coulomb counting and normal characterization.
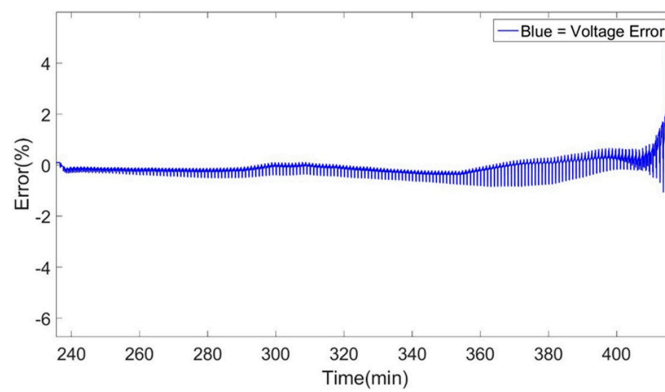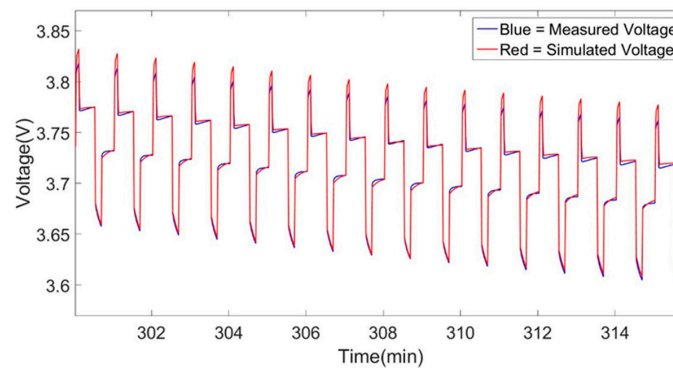
Table 5. Results of the models where the SoC window is less than the proposed error.

Temperature	SoC Window	⩽Error
15 °C	100%–16%	±2%
25 °C	100%–10%	±2%
35 °C	100%–12%	±2%
45 °C	100%–5%	±2%

3.2.2. 1st Order Thevenin Model with Advanced Characterization

Figure 13. 1st order Thévenin model measured and simulated DDP comparison at 25 °C with Coulomb counting and advanced characterization.

Figure 14. Error of the 1st Order Thévenin model measured and simulated DDP comparison at 25 °C with Coulomb counting and advanced characterization.
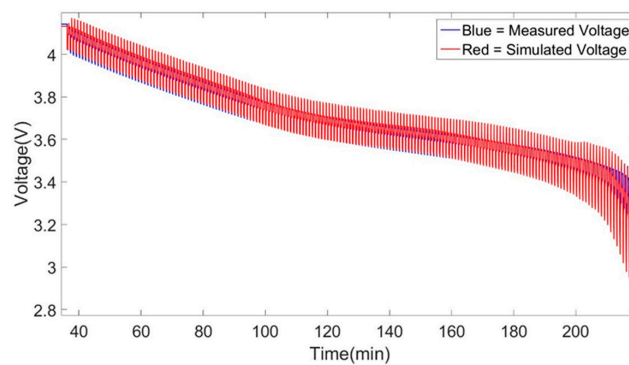

Figure 15. Dynamic behavior of the 1st order Thévenin Model measured and simulated DDP comparison at 25 °C with Coulomb counting and advanced characterization.
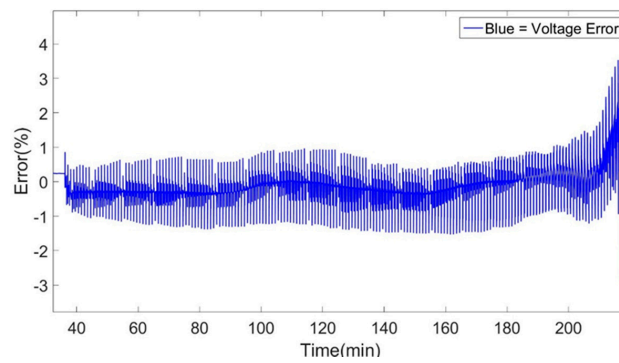
Table 6. Results of the models where the SoC window is less than the proposed error.

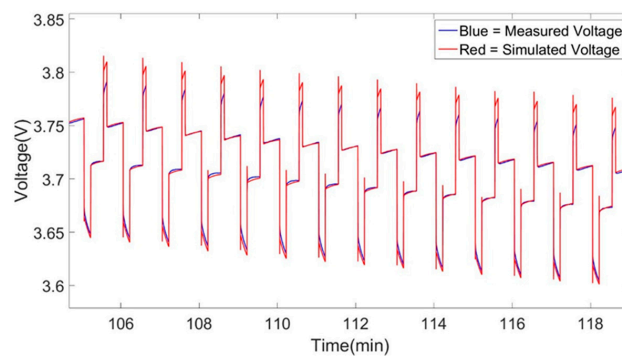| Temperature	SoC Window	⩽Error
15 °C	100%–9%	±2%
25 °C	100%–7%	±2%
35 °C	100%–10%	±1%
45 °C	100%–4%	±1%

3.2.3. 2nd Order Thévenin Model with Advanced Characterization

Figure 16. 2nd order Thévenin model measured and simulated DDP comparison at 25 °C with Coulomb counting and advanced characterization.

Figure 17. Error of the 2nd order Thévenin model measured and simulated DDP comparison at 25 °C with Coulomb counting and advanced characterization.
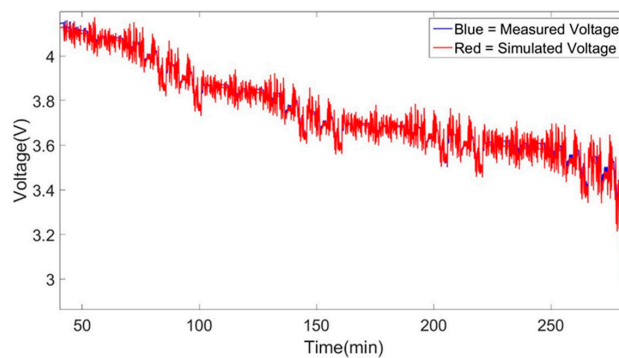

Figure 18. Dynamic behavior of the 2nd order Thévenin model measured and simulated DDP comparison at 25 °C with Coulomb counting and advanced characterization.

Table 7. Results of the models where the SoC window is less than the proposed error.

| Temperature	SoC Window	⩽Error
15 °C	100%–5%	±2%
25 °C	100%–0%	±2%
35 °C	100%–3%	±1%
45 °C	100%–0%	±1%

3.2.4. 2nd Order Thévenin Model with Advanced Characterization Validated under Worldwide Harmonized Light Vehicle Test Procedure Profile

Figure 19. 2nd order Thévenin model measured and simulated worldwide harmonized light vehicle test procedure (WLTC) comparison at 25 °C with Coulomb counting and advanced characterization.
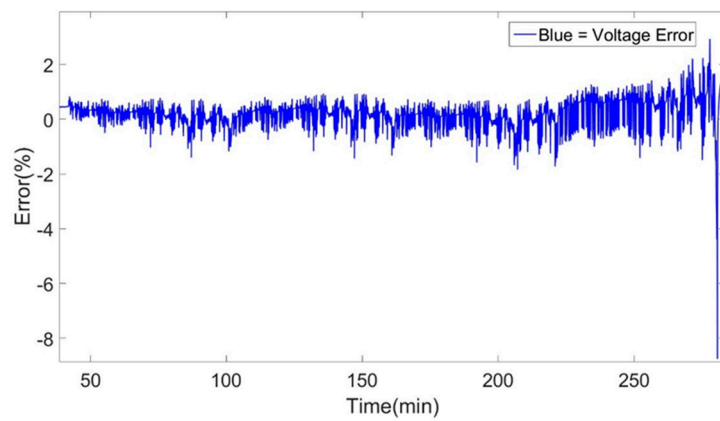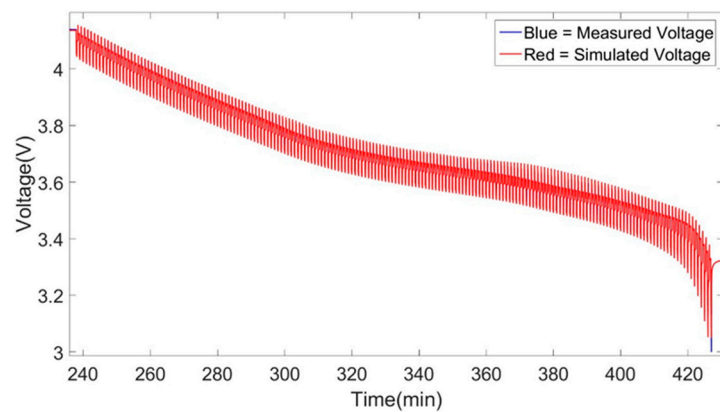
Figure 20. Error of the 2nd order Thévenin model measured and simulated WLTC comparison at 25 °C with Coulomb counting and advanced characterization.
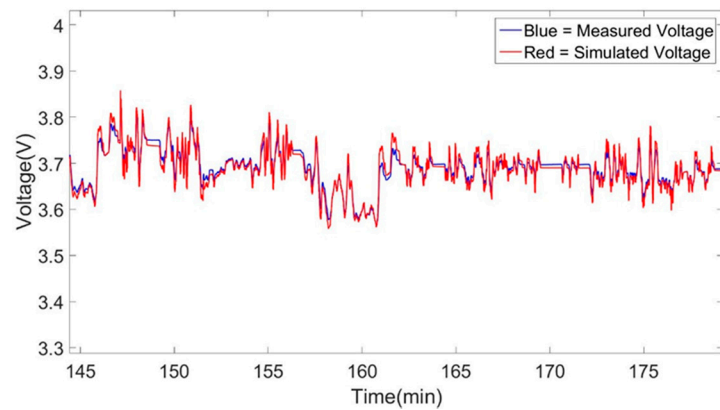
Figure 21. Dynamic behavior of the 2nd order Thévenin model measured and simulated WLTC comparison at 25 °C with Coulomb counting and advanced characterization.

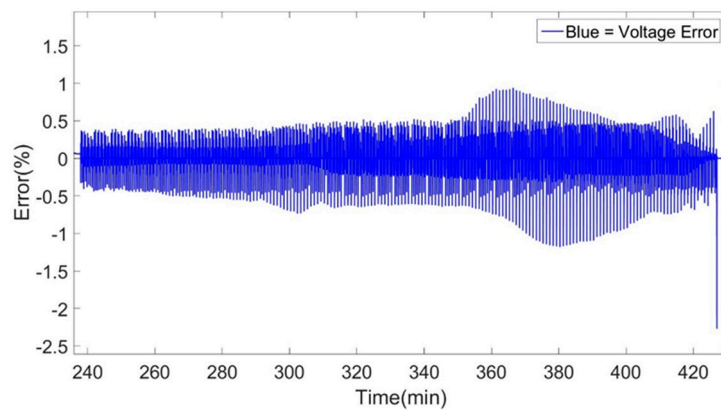3.2.5. 2nd Order Thévenin Model with Advanced Characterization Extended Kalman Filtering Technique
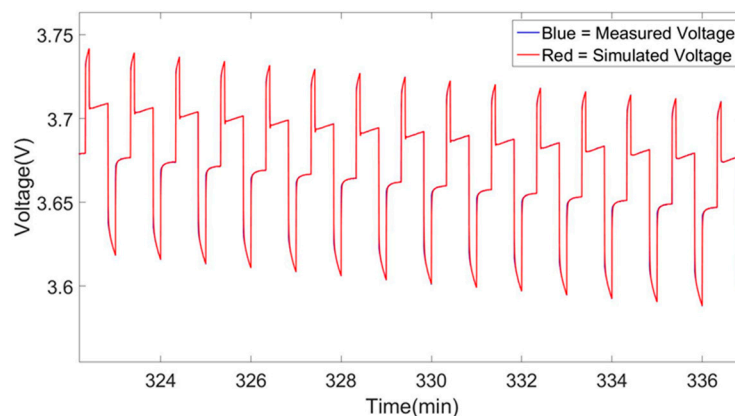

Figure 22. 2nd order Thévenin model measured and simulated DDP comparison at 25 °C with advanced Kalman filtering and advanced characterization.

Figure 23. Error of the 2nd order Thévenin model measured and simulated DDP comparison at 25 °C with advanced Kalman filtering and advanced characterization.

Table 8. Results of the models where the SoC window is less than the proposed error.

Temperature	SoC Window	⩽Error
15 °C	100%–15%	±2%
25 °C	100%–7%	±2%
35 °C	100%–8%	±2%
45 °C	100%–4%	±2%

Figure 24. Dynamic behavior of the 2nd order Thévenin model measured and simulated DDP comparison at 25 °C with advanced Kalman filtering and advanced characterization.

4. Discussion

Examining the 2nd order Thévenin parameters compared in Section 3, a clear difference can be observed between the values corresponding to the fresh cell BoL and to the aged cell (90% SoH). The loss of total capacity throughout the lifetime of the NMC cells and the difference in the model parameters between a fresh BoL and aged (90% SoH) cell can be explained by different degradation mechanisms which are mainly due to structural changes in the cell, the chemical composition or dissolution reaction and surface film modifications [59,66,67]. The degradation mechanisms can be separated into:

- Loss of lithium inventory (LLI);
- Loss of active material (LAM);
- Increase of the solid electrolyte interphase (SEI) layer.

The values of Ro, Rp and Rp2 are higher for the aged cell (90% SoH) than the values corresponding to the fresh cell BoL in contrast to the time constant values τ, where the fresh cell BoL values are slightly higher than the aged cell (90% SoH) values. We observed a mean difference of 71.3% at the 100% SoC value and 61% of the 0% SoC value for the charge and discharge parameters of Ro and Rp, while 59.4% at the 100% SoC value and 43% at the 0% SoC value of the charge and discharge parameters of Rp2. For the total time constants, we observed a mean difference of 24.07% at the 100% SoC value and 13.33% at the 0% SoC value. The behavior of the internal resistance of the model and the time constant of the models RC's branches was as expected. In this analysis we have considered the total time constant (τ_1 and τ_2) which are directly related with the total relaxation time of the cell. As a cell gets aged it is expected to see an increase in internal resistance due to the increased cycling numbers where lithium ions are intercalated between the anode and the cathode of the cell which increases the SEI layer, degrades the active materials (LLI and LAM) and decompose the electrolyte [68]. Additionally, it is also expected that an aged cell has a smaller relaxation time than a new cell due to the formation of definite structure inside the cell including the anode, electrolyte and cathode, thus explaining the lower values for the total time constants (τ_1 and τ_2) parameter at 95% and 90% SoH when observing them in Figure 8a,b [66].

It can be concluded that even if the values of the total time constants are lower for an aged compared to a new cell, thus having a faster behavior during relaxation phases, it is compensated by the high increase of the internal resistance values R_o, R_p and R_{p2}. This high increase of internal resistance is due to the different degradation mechanisms explained earlier. These effects can be also observed in the decreasing of the capacity value of the cell during its lifetime as seen in Figure 3 [69,70].

Additionally, we observe the difference of the total time constant values (τ_1 and τ_2) at low SoC to respect the values at high SoC this can be explain as follow. When observing the relaxation phases after a specific current pulse at low SoC we see a faster saturation of the voltage measured to the rest Voltage value than what we observe in the middle or high SoC values. This can explain why we have lower Tau values at low SoC's and higher at higher SoC's. Meaning that we have a faster relaxation at low SoC's than at high SoC's. This is the opposite for the internal resistance as we can observe at Figure 5 where we have higher internal resistance R_o at low SoC and lower R_o at high SoC's.

Parameters like the ones described above were also calculated for other temperatures at BoL. Those parameters were used to create the models described in Section 3.2 while additional parameters were created for the other temperatures under investigation. Observing the results of Section 3.2 some general observations regarding the comparison of the simulated to the measured results of the models can be mentioned:

- Increasing the temperature condition will create more efficient NMC lithium ion ECM models;
- Complex ECM topologies will increase the accuracy of NMC lithium-ion ECM models;
- Alter SoC estimation techniques to more complex will increase the accuracy of NMC lithium-ion ECM models;
- The models created can co-op with more dynamic profiles, like the WLTC profile.

The main condition that is predominantly affecting the accuracy of the models is the temperature. This effect can be observed on all topologies, for both types of characterization results used and for both the Coulomb counting and the extended Kalman filtering SoC estimation technique. This phenomenon can be explained by the fact that when performing the characterization tests at a higher temperature value, the different parts of the cell becomes more homogeneous, making the behavior of the cell during this condition more pronounced compared to that at lower temperatures. Thus, when creating parameters from these tests, the models will have less non-linear errors during the simulation. Moreover, when increasing the temperature condition, an increase in available capacity of the cell is observed, as shown in Figure 25.
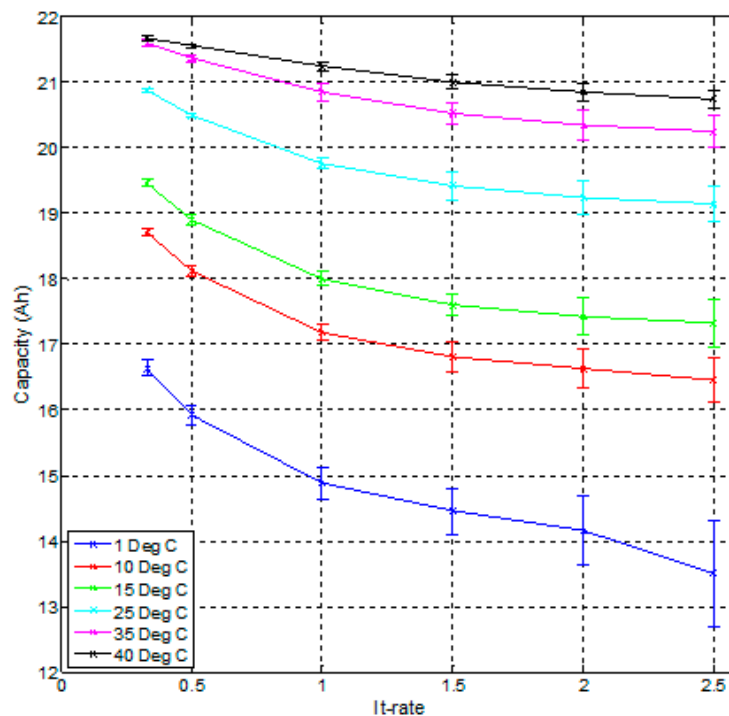
Figure 25. Discharge capacity evolution at different temperatures and different C-rates of NMC 20 Ah lithium ion cells.

Thus, when creating the parameters for these high temperatures, we have a better match between the energy used during our HPPC test (characterization test for the creation of R_o, R_p, R_{p2} and τ parameters) and the energy used during our DDP validation test. The increasing mismatch occurring at lower temperatures between the energy used, together with increasing time step of the simulation have been identified as sources of increasing errors during the simulation.

The main errors that have been encountered during the simulations can be identified at the high and low SoC window of the simulations. This effect as described above is minimized when increasing the temperature condition at which the models were created. Moreover, a clear improvement is observed in the models when changing the topology of the models from 1st to 2nd order Thévenin model. This effect can be observed between the 1st and 2nd order Thévenin model at 25 °C models while also at the others temperatures. The 1st order Thévenin model at 25 °C using advanced characterization datasets has identical accuracy as the 2nd order Thévenin model at 25 °C using advanced characterization datasets. But we see that the high and low SoC errors of the 2nd order Thévenin model is less pronounced specifically for the discharge behavior of the cell while there isn't any increase in high errors (4%), as the 1st order Thevenin mdoel, at the very end of the simulation.

Inspecting the 2nd order Thévenin models with Coulomb counting and extended Kalman filtering SoC estimation technique we observe a clear improvement in the accuracy of the model. Due to the extended method used by Kalman filtering to re-calculate and actualize the SoC of the cell in the model, the accuracy of our models is increased while we observed a clear improvement in the dynamic representations of the models presented in Figure 18. Comparing the 1st order models created with normal characterization and advance characterization datasets we observed that the accuracy of the models is increased but is not substantial as it is when changing temperature, topologies and SoC estimation techniques. Furthermore, the dynamic behavior has been affected more than the total accuracy of these models by the change of the characterization datasets from normal to advanced.

Collecting all these observations the model that should have created the best simulation accuracy and dynamic behaviors during the simulation should be models that are at high temperatures with complex topologies. In this regard, the most efficient model created for this study was the 2nd

order Thévenin model with advanced characterization datasets and extended Kalman filtering SoC estimation technique at 45 °C. Future work will investigate more in depth the development of ECM models based on a high number of cells creating average parameters for a batch of cells and comparing them to average validations profiles provided by the combination of the validations results (average DDP and WLTC profiles for a batch of cells). This analysis will provide a better understanding of the behavior of a set of NMC cells which represents with higher fidelity the situation observed in an automotive battery pack combined with a BMS.

Additionally, in future publications, the incorporation of in-depth analysis of the simulation time needed to run such models in a specific CPU-based platform (*i.e.*, automotive on-board computer) will be provided. Performing a preliminary investigation, it can be observed that the more complex the topology and extensive the parameters are, the longer it takes for a computer system to run the model. This time is in the order of 1 minute for the 1st and 2nd order Thevenin model combined with Coulomb counting SoC estimation technique. In contrast, with the use of the extended Kalman filtering where the computer system has to acquire and input the SoC values while he simulates the validation profile, we can observe a substantial increase in the simulation time needed to run the model. This time is in the order of 5 minutes. These simulations were performed by a computer with a Central Processing Unit (CPU) at 2.8 Ghz, with 16 GB Memory and a NVIDIA (Santa Clara, CA, USA) Quadro K2 100 M graphic card.

5. Conclusions

The proper simulation of lithium-ion batteries in today's automotive and electric applications is of great important for an efficient use and correct understanding of the electrical, thermal, chemical behavior of the system under investigation. Different models exist in the industry and literature, each having their own advantages and disadvantages. ECMs are mainly used in electrical lithium ion battery models for the simulation of the electrical and thermal behavior of the cell. The 1st and 2nd order Thévenin model are used to simulate a large format and high energy NMC lithium-ion battery with a capacity of 20 Ah for different temperatures. The models are created by using the Coulomb counting and the extended Kalman Filter SoC estimations and different type of validation profiles like the dynamic discharge pulse (DDP) and world harmonized light duty profiles were taken into account. Moreover, a different set of parameters were created based on two types of characterization tests performed (normal and advanced characterization). The creation of aged parameters was also developed based on the same characterization tests procedures and they were compared to the BoL parameters used in the parameterization of the ECM models. The behavior of the aged parameters with respect to the BoL were as expected mainly observing higher internal resistances for a battery cell that has aged *versus* a fresh cell while an opposite relation was observed for the total time constant τ (τ_1 and τ_2), with higher values for a fresh cell than a cell that has aged.

The temperature condition, the models were created, has a great effect on the validation results. The higher the temperature at which the characterization tests were performed, the more accurate the parameters are, providing a better validation result of the model. The difference in the topology of the 1st and 2nd order Thévenin model while the difference between the normal and advanced characterization test methods will decrease the error of the validation results but mainly they will allow for better dynamic representations and less linear errors at high and low SoC levels of the cell. The 2nd order Thévenin model at 45 °C with advanced characterization and extended Kalman filtering is found to be the most accurate model.

Abbreviations

BEV	Battery electric vehicle
BMS	Battery management system
BoL	Begin of life
CUP	Central Processing Unit
DDP	Dynamic discharge dynamic pulse test
ECM	Equivalent circuit models
EIS	Electrical impedance spectroscopy
EoL	End of life
EREV	Extended range electric vehicle
HEV	Hybrid electric vehicle
HPPC	High pulse power characterization test
ICE	Internal combustion engine
LAM	Loss of active material
LLI	Loss of lithium inventory
NMC	Nickel manganese cobalt
OCV	Open circuit voltage
PEV	Plug-in electric vehicle
PHEV	Plug-in hybrid electric vehicle
PNGV	Partnership for a new generation of vehicles
RC	Combination of resistances and capacitance
SEI	Solid electrolyte interphase
SoC	State of charge
SoH	State-of-health
WLTC	Worldwide harmonized light vehicle test procedure

References

1. Hu, X.; Li, S.; Peng, H. A comparative study of equivalent circuit models for Li-ion batteries. *J. Power Sources* **2012**, *198*, 359–367. [CrossRef]
2. He, H.; Xiong, R.; Guo, H.; Li, S. Comparison study on the battery models used for the energy management of batteries in electric vehicles. *Energy Convers. Manag.* **2012**, *64*, 113–121. [CrossRef]
3. Ramadesigan, V.; Northrop, P.W.C.; De, S.; Santhanagopalan, S.; Braatz, R.D.; Subramanian, V.R. Modeling and simulation of lithium-ion batteries from a systems engineering perspective. *J. Electrochem. Soc.* **2012**, *159*, R31–R45. [CrossRef]
4. Chen, M.; Member, S.; Rinc, G.A. Accurate electrical battery model capable of predicting runtime and I-V performance. *IEEE Trans. Energy Convers.* **2006**, *21*, 504–511. [CrossRef]
5. Feng, J.; He, Y.L.; Wang, G.F. Comparison study of equivalent circuit model of Li-Ion battery for electrical vehicles. *Res. J. Appl. Sci. Eng. Technol.* **2013**, *6*, 3756–3759.
6. Martínez-Rosas, E.; Vasquez-Medrano, R.; Flores-Tlacuahuac, A. Modeling and simulation of lithium-ion batteries. *Comput. Chem. Eng.* **2011**, *35*, 1937–1948. [CrossRef]
7. Thanagasundram, S.; Arunachala, R.; Makinejad, K.; Teutsch, T.; Jossen, A. A Cell Level Model for Battery Simulation. In Proceedings of the European Electric Vehicle Congress, Brussels, Belgium, 22 November 2012; pp. 1–13.
8. Johnson, V.H. Battery performance models in ADVISOR. *J. Power Sources* **2002**, *110*, 321–329. [CrossRef]

9.　He, H.; Xiong, R.; Fan, J. Evaluation of lithium-ion battery equivalent circuit models for state of charge estimation by an experimental approach. *Energies* **2011**, *4*, 582–598. [CrossRef]

10.　Rahmoun, A.; Biechl, H. Modelling of Li-ion batteries using equivalent circuit diagrams. *Przeglad Elektrotechniczny* **2012**, *88*, 152–166.

11.　González-longatt, F.M. Circuit Based Battery Models: A Review. In Proceedings of the 2nd Congreso IberoAmericano De Estudiantes de Ingenieria Electrica, Puerto la Cruz, Venezuela, 15 April 2006.

12.　Johnson, V.H.; Pesaran, A.A.; Sack, T. *Temperature-Dependent Battery Models for High-Power Lithium-Ion Batteries*; US Department of Energy, National Renewable Energy Laboratory: Golden, CO, USA, 2001.

13.　Einhorn, M.; Conte, F.V.; Kral, C.; Member, S. Comparison, selection, and parameterization of electrical battery models for automotive applications. *IEEE Trans. Power Electron.* **2013**, *28*, 1429–1437. [CrossRef]

14.　Daowd, M.; Omar, N.; Verbrugge, B.; Van Den Bossche, P.; Van Mierlo, J. Battery Models Parameter Estimation based on Matlab/Simulink®. In Proceedings of the 25th Electric Vehicle Symposium (EVS-25), Shenzhen, China, 5–9 November 2010; Volume 59.

15.　Zhang, C.; Liu, J.; Sharkh, S.M.; Zhang, C. Identification of Dynamic Model Parameters for Lithium-Ion Batteries used in Hybrid Electric Vehicles. In Proceedings of the International Symposium on Electric Vehicles (ISEV), Beijing, China, September 2009; p. 11.

16.　Plett, G.L. Extended Kalman filtering for battery management systems of LiPB-based HEV battery packs. *J. Power Sources* **2004**, *134*, 262–276. [CrossRef]

17.　Belt, J.R. *Battery Test Manual for Plug-In Hybrid Electric Vehicles*; U.S. Department of Energy: Idaho, ID, USA, March 2008.

18.　*FreedomCAR Battery Test Manual For Power-Assist Hybrid Electric Vehicles Disclaimer*; U.S. Deparment of Energy: Idaho, ID, USA, October 2003.

19.　Daowd, M.; Omar, N.; Van Mierlo, J.; Van Den Bossche, P. *An Extended PNGV Battery Model for Electric and Hybrid Vehicles Abbreviations or Glossary*; International Review of Electrical Engineering: Brussels, Belgium, 15 June 2011.

20.　Omar, N.; Daowd, M. Assessment of second life of lithium iron phosphate based batteries. *Int. Rev. Electr. Eng.* **2012**, *7*, 3941.

21.　Hegazy, O.; Affiliations, C. *Series Hybrid Electric Vehicles*; Encyclopedia of Automotive Engineering: Brussels, Belgium, 29 April 2014.

22.　Van Mierlo, J.; Hegazy, O. *Parallel Hybrid Electric Vehicles*; Encyclopedia of Automotive Engineering: Brussels, Belgium, 29 April 2014; Chapter 59; p. 1067.

23.　Omar, N.; Daowd, M.; Hegazy, O.; Mulder, G.; Timmermans, J.-M.; Coosemans, T.; Van Den Bossche, P.; Van Mierlo, J. Standardization work for BEV and HEV applications: Critical appraisal of recent traction battery documents. *Energies* **2012**, *5*, 138–156. [CrossRef]

24.　Pesaran, A.A.; Kim, G.-H.; Keyser, M. Integration Issues of Cells into Battery Packs for Plug-In and Hybrid Electric Vehicles. In Proceedings of the Hybrid and Fuel Cell Electric Vehicle Symposium on EVS-24 International Battery, Stavanger, Norway, 13–16 May 2009.

25.　*Battery Pack Design, Validation, and Assembly Guide using A123 Systems AMP20M1HD—A Nanophosphate® Cells*; A123 Systems: MI, USA, 7 February 2014; pp. 1–71.

26.　Yen, E.; Han, T.; Kher, S. Automating battery pack design. *ANSYS Advant.* **2015**, *IX*, 18–21.

27.　Group Energy Innovation. Available online: http://www.eigbattery.com (accessed on 13 April 2016).

28.　Nikolian, A.; De Hoog, J.; Fleurbay, K.; Timmermans, J.; Van de Bossche, P.; Van Mierlo, J. Classification of Electric Modelling and Characterization Methods of Lithium-Ion Batteries for Vehicle Applications. In Proceedings of the European Electric Vehicle Congress, Brussels, Belgium, 4 December 2014; pp. 1–15.

29.　Kutílek, M.; Jendele, L.; Krejca, M. Comparison of empirical, semi-empirical and physically based models of soil hydraulic functions derived for bi-modal soils. *J. Contam. Hydrol.* **2009**, *104*, 84–89. [CrossRef] [PubMed]

30.　Jongerden, M.; Haverkort, B. Battery Modeling. 2008. Available online: http://doc.utwente.nl/64866/1/battery-model.pdf (accessed on 7 May 2016).

31.　Omar, N.; Bossche, P.; Coosemans, T.; Mierlo, J. Peukert revisited—critical appraisal and need for modification for lithium-ion batteries. *Energies* **2013**, *6*, 5625–5641. [CrossRef]

32.　Smekens, J.; Paulsen, J.; Yang, W.; Omar, N.; Deconinck, J.; Hubin, A.; Van Mierlo, J. A Modified Multiphysics model for lithium-ion batteries with a $Li_xNi_{1/3}Mn_{1/3}Co_{1/3}O_2$ electrode. *Electrochim. Acta* **2015**, *174*, 615–624. [CrossRef]

33. Rahman, M.A.; Anwar, S.; Izadian, A. Electrochemical model parameter identification of a lithium-ion battery using particle swarm optimization method. *J. Power Sources* **2016**, *307*, 86–97. [CrossRef]

34. Smekens, J.; Omar, N.; Hubin, A.; Van Mierlo, J.; Van Den Bossche, P. Optimization of Li-Ion Batteries through Modelling Techniques. In Proceedings of the EVS28 International Electric Vehicle Symposium and Exhibition, Kintex, Korea, 3–6 May 2015.

35. Doyle, M. Modeling of galvanostatic charge and discharge of the lithium/polymer/insertion cell. *J. Electrochem. Soc.* **1993**, *140*, 1526–1533. [CrossRef]

36. Fuller, T.F.; Doyle, M.; Newman, J. Simulation and optimization of the dual lithium ion insertion cell. *J. Electrochem. Soc.* **1994**, *141*, 1–10. [CrossRef]

37. He, H.; Zhang, X.; Xiong, R.; Xu, Y.; Guo, H. Online model-based estimation of state-of-charge and open-circuit voltage of lithium-ion batteries in electric vehicles. *Energy* **2012**, *39*, 310–318. [CrossRef]

38. Smekens, J.; Hegazy, O.; Omar, N.; Widanage, D.; Hubin, A.; Van Mierlo, J.; Van Den Bossche, P. Influence of Pulse Variations on the Parameters of First Order Empirical Li-Ion Battery Model. In Proceedings of the 2013 World Electric Vehicle Symposium and Exhibition (EVS27), Barcelona, Spain, 17–20 November 2013; pp. 1–6.

39. Lu, L.; Han, X.; Li, J.; Hua, J.; Ouyang, M. A review on the key issues for lithium-ion battery management in electric vehicles. *J. Power Sources* **2013**, *226*, 272–288. [CrossRef]

40. Tremblay, O.; Dessaint, L.-A.; Dekkiche, A.-I. A Generic Battery Model for the Dynamic Simulation of Hybrid Electric Vehicles. In Proceedings of the 2007 IEEE Vehicle Power and Propulsion Conference, Arlington, TX, USA, 9–12 September 2007; pp. 284–289.

41. Omar, N.; Verbrugge, B.; Mulder, G.; Van Den Bossche, P.; Van Mierlo, J.; Daowd, M. Evaluation of Performance Characteristics of Various Lithium-Ion Batteries for Use in BEV Application. In Proceedings of the 2010 IEEE Vehicle Power and Propulsion Conference, Lille, France, 1–3 Sepember 2010; pp. 1–6.

42. Omar, N.; Daowd, M.; Van Den Bossche, P.; Hegazy, O.; Smekens, J.; Coosemans, T.; Van Mierlo, J. Rechargeable energy storage systems for plug-in hybrid electric vehicles—Assessment of electrical characteristics. *Energies* **2012**, *5*, 2952–2988. [CrossRef]

43. Einhorn, M.; Conte, V.F.; Kral, C.; Fleig, J.; Permann, R. Parameterization of an Electrical Battery Model for Dynamic System Simulation in Electric Vehicles. In Proceedings of the 2010 IEEE Vehicle Power and Propulsion Conference, Lille, France, 1–3 Sepember 2010; pp. 1–7.

44. Jackey, R.A. *A Simple, Effective Lead-Acid Battery Modeling Process for Electrical System Component Selection*; MathWorks Inc: Novi, MI, USA, 2007.

45. Omar, N.; Widanage, D.; Monem, A.M.; Firouz, Y.; Hegazy, O.; Van Den Bossche, P.; Coosemans, T.; Van Mierlo, J. Optimization of an advanced battery model parameter minimization tool and development of a novel electrical model for lithium-ion batteries. *Int. Trans. Electr. Energy Syst.* **2014**, *24*, 1747–1767. [CrossRef]

46. Standard IEC 62660-1. *Secondary Lithium-Ion Cells for the Propulsion of Electric Road Vehicles—Part 1: Performance Testing*; International Electrotechnical Commission: Geneva, Switzerland, 2010.

47. ISO 12405-1:2011. *Electrically Propelled Road Vehicles—Test Specification for Lithium-Ion Traction Battery Packs and Systems—Part 1: High-Power Applications*; International Organization for Standardization: Geneva, Switzerland, 2011.

48. ISO 12405-2. *Electrically Propelled Road Vehicles—Test Specification for Lithium-Ion Traction Battery Packs and Systems—Part 2: High energy application*; no. 20; International Organization for Standardization: Geneva, Switzerland, 2009.

49. IEC 61982-2. *Secondary Batteries for the Propulsion of Electric Road Vehicles—Part 2: Dynamic Discharge perFormance Test and Dynamic Endurance Test*; International Electrochemical Commission: Geneva, Switzerland, 2010.

50. Tang, X.; Mao, X.; Lin, J.; Koch, B. Li-Ion Battery Parameter Estimation for State of Charge. In Proceedings of the 2011 American Control Conference, San Francisco, CA, USA, 29 June–1 July 2011; pp. 941–946.

51. Sun, F.; Xiong, R.; He, H. Estimation of state-of-charge and state-of-power capability of lithium-ion battery considering varying health conditions. *J. Power Sources* **2014**, *259*, 166–176. [CrossRef]

52. Plett, G.L. Extended Kalman filtering for battery management systems of LiPB-based HEV battery packs: Part 1. Background. *J. Power Sources* **2004**, *134*, 252–261. [CrossRef]

53. Rahimi-eichi, H.; Member, S.; Chow, M. Adaptive Parameter Identification and State-of-Charge Estimation of Lithium- Ion Batteries Adaptive Parameter Identification and State-of-Charge Estimation of Lithium-Ion Batteries. In Proceedings of the 2014 17th International Conference on Electrical Machines and Systems (ICEMS), Hangzhou, China, 22–25 October 2012; pp. 855–860.

54. Berecibar, M.; Gandiaga, I.; Villarreal, I.; Omar, N.; Van Mierlo, J.; Van Den Bossche, P. Critical review of state of health estimation methods of Li-ion batteries for real applications. *Renew. Sustain. Energy Rev.* **2016**, *56*, 572–587. [CrossRef]

55. Waag, W.; Fleischer, C.; Uwe Sauer, D. Critical review of the methods for monitoring of lithium-ion batteries in electric and hybrid vehicles. *J. Power Sources* **2014**, *258*, 321–339. [CrossRef]

56. Plett, G.L. Sigma-point Kalman filtering for battery management systems of LiPB-based HEV battery packs. *J. Power Sources* **2006**, *161*, 1369–1384. [CrossRef]

57. Fang, H.; Wang, Y.; Sahinoglu, Z.; Wada, T.; Hara, S. State of charge estimation for lithium-ion batteries: An adaptive approach. *Control Eng. Pract.* **2014**, *25*, 45–54. [CrossRef]

58. Liu, G.; Ouyang, M.; Lu, L.; Li, J.; Hua, J. A highly accurate predictive-adaptive method for lithium-ion battery remaining discharge energy prediction in electric vehicle applications. *Appl. Energy* **2015**, *149*, 297–314. [CrossRef]

59. Barré, A.; Deguilhem, B.; Grolleau, S.; Gérard, M.; Suard, F.; Riu, D. A review on lithium-ion battery ageing mechanisms and estimations for automotive applications. *J. Power Sources* **2013**, *241*, 680–689. [CrossRef]

60. Seaman, A.; Dao, T.-S.; McPhee, J. A survey of mathematics-based equivalent-circuit and electrochemical battery models for hybrid and electric vehicle simulation. *J. Power Sources* **2014**, *256*, 410–423. [CrossRef]

61. He, H.; Liu, Z.; Hua, Y. Adaptive extended kalman filter based fault detection and isolation for a lithium-ion battery pack. *Energy Procedia* **2015**, *75*, 1950–1955. [CrossRef]

62. Dai, H.; Zhu, L.; Zhu, J.; Wei, X.; Sun, Z. Adaptive Kalman filtering based internal temperature estimation with an equivalent electrical network thermal model for hard-cased batteries. *J. Power Sources* **2015**, *293*, 351–365. [CrossRef]

63. *IEC 62660-2: Secondary Lithium-Ion Cells for the Propulsion of Electric Road Vehicles—Part 2: Reliability and Abuse Testing*; International Electrochemical Commission: Geneva, Switzerland, 2010.

64. Huria, T.; Ceraolo, M.; Gazzarri, J.; Jackey, R. High Fidelity Electrical Model with Thermal Dependence for Characterization and Simulation of High Power Lithium Battery Cells. In Proceedings of the 2012 IEEE International Electric Vehicle Conference, Greenville, SC, USA, 4–8 Mach 2012; pp. 1–8.

65. Schweiger, H.G.; Obeidi, O.; Komesker, O.; Raschke, A.; Schiemann, M.; Zehner, C.; Gehnen, M.; Keller, M.; Birke, P. Comparison of several methods for determining the internal resistance of lithium ion cells. *Sensors* **2010**, *10*, 5604–5625. [CrossRef] [PubMed]

66. Berecibar, M.; Omar, N.; Garmendia, M. SOH Estimation and Prediction for NMC Cells Based on Degradation Mechanism Detection. In Proceedings of the 2015 IEEE on Vehicle Power and Propulsion Conference (VPPC), Montreal, QC, Canada, 19–22 October 2015; pp. 1–6.

67. Vetter, J.; Novák, P.; Wagner, M.R.; Veit, C.; Möller, K.-C.; Besenhard, J.O.; Winter, M.; Wohlfahrt-Mehrens, M.; Vogler, C.; Hammouche, A. Ageing mechanisms in lithium-ion batteries. *J. Power Sources* **2005**, *147*, 269–281. [CrossRef]

68. Omar, N.; Firouz, Y.; Gualous, H.; Salminen, J.; Kallio, T.; Timmermans, J.M.; Coosemans, T.; Van den Bossche, P.; Van Mierlo, J. *Aging and degradation of lithium-ion batteries*; Woodhead Publishing Limited: Cambridge, UK, 2015; pp. 263–279.

69. Dubarry, M.; Svoboda, V.; Hwu, R.; Liaw, B.Y. Capacity and power fading mechanism identification from a commercial cell evaluation. *J. Power Sources* **2007**, *165*, 566–572. [CrossRef]

70. Liaw, B.Y.; Jungst, R.G.; Nagasubramanian, G.; Case, H.L.; Doughty, D.H. Modeling capacity fade in lithium-ion cells. *J. Power Sources* **2005**, *140*, 157–161. [CrossRef]